Published in final edited form as:
Mol Cell. 2008 May 23; 30(4): 403–414. doi:10.1016/j.molcel.2008.03.009.

The CUL7 E3 Ubiquitin Ligase Targets Insulin Receptor Substrate 1 for Ubiquitin-Dependent Degradation

Xinsong Xu[1,4], **Antonio Sarikas**[1,4], **Dora C. Dias-Santagata**[1,5], **Georgia Dolios**[2], **Pascal J. Lafontant**[3], **Shih-Chong Tsai**[3], **Wuqiang Zhu**[3], **Hidehiro Nakajima**[3], **Hisako O. Nakajima**[3], **Loren J. Field**[3], **Rong Wang**[2], and **Zhen-Qiang Pan**[1,*]

1*Department of Oncological Sciences, The Mount Sinai School of Medicine, New York, NY 10029-6574, USA*

2*Department of Genetics and Genomic Sciences, The Mount Sinai School of Medicine, New York, NY 10029-6574, USA*

3*Indiana University School of Medicine, Wells Center for Pediatric Research and Krannert Institute of Cardiology, Indianapolis, IN 47202-5225, USA*

SUMMARY

Recent genetic studies have documented a pivotal growth-regulatory role played by the Cullin 7 (CUL7) E3 ubiquitin ligase complex containing the Fbw8-substrate-targeting subunit, Skp1, and the ROC1 RING finger protein. In this report, we identified insulin receptor substrate 1 (IRS-1), a critical mediator of the insulin/insulin-like growth factor 1 signaling, as a proteolytic target of the CUL7 E3 ligase in a manner that depends onmammalian target of rapamycin and the p70 S6 kinase activities. Interestingly, while embryonic fibroblasts of *Cul7*$^{-/-}$ mice were found to accumulate IRS-1 and exhibit increased activation of IRS-1's downstream Akt and MEK/ERK pathways, these null cells grew poorly and displayed phenotypes reminiscent of those associated with oncogene-induced senescence. Taken together, our findings demonstrate a key role for the CUL7 E3 in targeting IRS-1 for degradation, a process that may contribute to the regulation of cellular senescence.

INTRODUCTION

Selective proteolytic degradation by the ubiquitin (Ub)-26S proteasome pathway effectively lowers concentration of a target protein in a timely fashion, thereby regulating numerous biological processes (Hershko and Ciechanover, 1998). A defining component of this pathway centers at the recognition of a substrate by an E3 Ub ligase, which also recruits an E2 Ub-conjugating enzyme. It is the concerted interactions between the bound substrate, the E3, and the Ub-charged E2 that yield polyubiquitinated target protein, which is then delivered to the 26S proteasome for proteolysis.

Of the cellular E3s, the cullin-RING finger multisubunit complexes are the largest family, characterized by two signature components: a cullin (CUL) family molecule containing a conserved cullin domain, and its RING finger partner ROC1/Rbx1/Hrt1 (Petroski and Deshaies, 2005). Cullins are molecular scaffolds that organize reactive modules to coordinate substrate ubiquitination. In the prototypic Skp1•CUL1•F box protein-ROC1 (SCF) E3, CUL1 is bound to both an Skp1•F box protein module and a ROC1 RING-based Ub core ligase, thereby placing the F box protein (member of a large family of substrate targeting molecules)

*Correspondence: zhen-qiang.pan@mssm.edu.
[4]These authors contributed equally to this work
[5]Present address: Massachusetts General Hospital, Boston, MA 02115, USA.

within the proximity of ROC1, which recruits an E2-conjugating enzyme to allow for the transfer of Ub to the optimally positioned substrate.

A large noncanonical cullin composed of nearly 1700 amino acids, CUL7 (also named p193 or p185), assembles a SCF-like E3 complex containing Skp1, the Fbw8 F-box protein (also called Fbx29), and ROC1 (Dias et al., 2002; Arai et al., 2003; Tsunematsu et al., 2006). Unlike CUL1, CUL7 does not bind the Skp1 adaptor alone but selectively interacts with the Skp1•Fbw8 heterodimer (Dias et al., 2002). Recently, Cormier-Daire and colleagues have linked the 3-M syndrome, which is characterized by pre- and postnatal growth retardation, to *Cul7* germline mutations, a majority of which have been implicated for loss of the functional cullin domain (Huber et al., 2005). Consistent with this finding, a more recent report has identified a common *Cul7* germline mutation that may be responsible for the Yakuts short stature syndrome (Maksimova et al., 2007). Moreover, mice studies have revealed that deletion of either *Cul7* (Arai et al., 2003) or *Fbw8* (Tsunematsu et al., 2006; Tsutsumi et al., 2008) causes profound intrauterine growth retardation. Taken together, the emerging genetic evidence has strongly suggested a pivotal role for the CUL7 E3 ligase in growth control.

CUL7 may have additional functions that include transformation mediated by simian virus-40 (SV40) large T antigen (Kohrman and Imperiale, 1992; Daud et al., 1993; Kasper et al., 2005), apoptosis (Tsai et al., 2000; Kim et al., 2007), p53 regulation (Andrews et al., 2006; Dowell et al., 2007; Kaustov et al., 2007; Jung et al., 2007), and the degradation of cyclin D1 (Okabe et al., 2006).

In this study, we report the identification of insulin receptor substrate 1 (IRS-1), a critical mediator of the insulin/insulin-like growth factor 1 (IGF-1)-signaling system (Dearth et al., 2007), as a proteolytic target of the CUL7 E3 and a requirement for mammalian target of rapamycin (mTOR) in this degradation process. In addition, we showed that embryonic fibroblasts derived from *Cul7*$^{-/-}$ mice contained elevated levels of IRS-1 and exhibited phenotypes that resemble those associated with oncogene-induced senescence.

RESULTS

The CUL7 E3 Ligase Targets IRS-1 for Degradation

To search for proteolytic targets by the CUL7 E3, we employed a proteomic approach to isolate and identify cellular proteins that were coimmunoprecipitated with Flag-Fbw8, the substrate-targeting subunit of the E3 complex, which was expressed constitutively in a HEK293-derived stable cell line (FF8HEK). While silver stain (Figure 1A) and immunoblot (Figure 1B) analyses confirmed previously demonstrated association between Fbw8, CUL7, Skp1, and ROC1 (Dias et al., 2002), screening for new Fbw8-associated proteins using mass spectrometry identified two peptides that matched human IRS-1 (Figure 1A).

Reciprocal coimmunoprecipitation experiments revealed interaction between V5-IRS-1 and Myc-Fbw8, which were ectopically expressed in HEK293 cells (Figure 1C, lane 3). Treatment with the proteasome inhibitor MG132 markedly enhanced this interaction (Figure 1C, lane 4). To assess the endogenous association, MCF-7 cell extracts were immunoprecipitated with anti-CUL7 monoclonal antibody, which detected copurification of CUL7 with Fbw8 and IRS-1 (Figure 1D). Of note, poor quality of anti-Fbw8 antibody precluded its use for probing endogenous interactions.

Immunoblot and coimmunoprecipitation experiments were performed to determine if Myc-Fbw8 influenced the steady-state level and polyubiquitination status of V5-IRS-1 in transfected HEK293 cells. As shown, Myc-Fbw8 decreased the expression of V5-IRS-1 (Figure 2A, compare lanes 1 and 4), which, however, was restored upon exposing the cells to MG132

(Figure 2A, lane 5), suggesting that Fbw8 promoted proteasomal degradation of IRS-1. In addition, coimmunoprecipitation and immunoblot analyses revealed the presence of high molecular weight HA-Ub conjugates in the V5-IRS-1 immunoprecipitates, which formed only in cells treated with MG132 (Figure 2A, lane 6), in a manner that was stimulated by overexpression of Fbw8 (lane 7). These results suggest that Fbw8 might promote formation of polyubiquitinated IRS-1, which was degraded by the proteasome rapidly.

To assess specificity, the aforementioned degradation analyses were performed with other F box proteins that include Skp2, βTrCP2, and Fbx22. These F box proteins, however, produced little, if any, effect on the steady-state level of V5-IRS-1 (Figure 2B). In addition, deletion of the F box domain in Fbw8, which reduces the association with Skp1 and hence CUL7 and ROC1 (Dias et al., 2002), decreased Fbw8's ability to induce the degradation of V5-IRS-1 (Figure 2B, lane 7), consistent with a requirement of the four-subunit CUL7 E3 for promoting proteolysis.

Finally, we measured the decay rate of IRS-1 in the absence of protein synthesis and asked whether it could be increased by overexpression of Fbw8 and CUL7. Cells (MCF-7) were transfected with empty vector or vectors overexpressing Fbw8 and CUL7 and then cultured in the presence of the protein synthesis inhibitor, cycloheximide (CHX), for a subsequent 6 hr period, over which IRS-1 protein decay was monitored. IRS-1 decayed very slowly (Figure 2C, lanes 1–3), in keeping with previously published observations (Shah et al., 2004). However, overexpression of Fbw8 and CUL7 markedly accelerated the decay rate of IRS-1 (Figure 2C, lanes 4–6; graph).

Collectively, the above results, combined with subsequent data using in vitro reconstitution assays (Figure 5), are consistent with a hypothesis that the CUL7 E3 ligase binds IRS-1, promotes its polyubiquitination and degradation by the 26S proteasome, and consequently shortens its half-life.

In humans, there are two close IRS-1 homologs: IRS-2 and IRS-4 (White, 2002). Our preliminary studies suggest that while Fbw8 promotes the degradation of IRS-4, it did not appear to interact with IRS-2 or to affect its stability (data not shown). The biochemical basis underlying this difference is presently unclear.

Fbw8-Mediated Degradation of IRS-1 Requires mTOR Activity

Ubiquitin-dependent degradation of IRS-1 is a cellular negative-feedback mechanism that attenuates the strength or duration of insulin/IGF-1/PI3-K activation (Harrington et al., 2005). This process requires PI3-K/Akt-dependent activation of the small G protein Rheb, which activates mTOR and its downstream effector kinase S6K (the p70 S6 kinase) that serine-phosphorylate IRS-1, thereby triggering its polyubiquitination and degradation (Harrington et al., 2005).

To assess whether Fbw8-mediated degradation of IRS-1 is a component of the abovementioned negative-feedback loop, we determined whether this proteolysis was sensitive to rapamycin, which inhibits mTOR, and whether it was stimulated by Rheb, which activates the kinase (Harrington et al., 2005). Consistent with previous observations (Figure 2C), MCF-7 cells, when overexpressing CUL7 and Fbw8, exhibited increased rate of IRS-1 degradation (Figure 3A, compare lanes 1–4 and lanes 5–8). However, exposure of the Flag-CUL7/Myc-Fbw8-expressing cells to rapamycin restored the stability of IRS-1 (Figure 3A, lanes 9–12; graph), indicating that Fbw8-mediated degradation of IRS-1 is inhibited by rapamycin.

We next examined the influence of Rheb on the steady state of IRS-1 in MCF-7 cells. While overexpression of either HA-Rheb (Figure 3B, lane 3) or Myc-Fbw8 (lane 2) reduced the levels

of endogenous IRS-1 only slightly, coexpression of Rheb and Fbw8 induced effective degradation of IRS-1 (lane 4). This finding suggests that both the Rheb and Fbw8 activities are limiting in MCF-7 cells. While forced expression of Rheb activates mTOR/S6K that in turn serine-phosphorylate IRS-1, elevated levels of Fbw8 promote the assembly of the CUL7 E3 ligase that mediates the ubiquitination of IRS1, leading to its proteasomal degradation.

Of note, V5-IRS-1 was readily degraded in HEK293 cells by overexpressing Fbw8 alone (Figures 2A and 2B). However, degradation of the endogenous IRS-1 in MCF-7 cells required over-expression of both Fbw8 and Rheb (Figure 3B). This discrepancy may be due to a difference in the magnitude of mTOR activity in different cell types under standard cell-culture conditions (10% FBS in DMEM). Consistent with this notion, while a substantial portion of V5-IRS-1 exists in slow-migrating, hyperphosphorylated forms in HEK293 cells (Figures 2A and 2B; verified in Figure S1A, available online), a majority of endogenous IRS-1 appeared in hypophosphorylated species in MCF-7 cells (Figure 2C, lane 1; Figure 3A, lane 1).

In all, these results suggest that degradation of IRS-1 by the CUL7 E3 requires mTOR activity and may serve as a critical step to restrain IGF-1/PI3-K signaling (Figure 3C; see the Discussion).

N-Terminal Half of IRS-1 Mediates Fbw8-Dependent Degradation

Previous studies have identified and implicated multiple mTOR/S6K phosphorylation sites in human IRS-1, including S307, S312, S527, and S636 (Harrington et al., 2004; Shah and Hunter, 2006). In order to gain insights into the degradation signals that direct Fbw8-mediated proteolysis of IRS-1, we performed both site-directed mutagenesis and deletion experiments. It was observed that a quintuple mutant V5-IRS-1^{5A} (in which S307/S312/S527/S636/S639 have been substituted with alanines), but not V5-IRS-1$^{S307A/S312A}$, V5-IRS-1^{S527A}, or V5-IRS-1$^{S636A/S639A}$, exhibited a partial resistance to degradation by Fbw8 (Figure 4A, compare lanes 2 and 5 and compare lanes 2, 8, 11, and 14). As shown, four IRS-1 C-terminally truncated proteins, spanning amino acids 1–268, 1–522, 1–574, or 1–626, respectively, were well expressed upon introduction into HEK293 cells (Figure 4B, lanes 4, 7, 10, and 13). Of these variants, V5-IRS-1 (1–574) and V5-IRS-1 (1–626) were the only two forms capable of mediating degradation induced by Fbw8 (lanes 11 and 14) in an MG132-reversible manner (lanes 12 and 15).

Collectively, the above results suggest that (1) IRS-1 contains the destruction signal that mediates Fbw8-imposed degradation, with its C-terminal boundary around position 574; (2) both V5-IRS-1 (1–574) and V5-IRS-1 (1–626) were extensively phosphorylated (Figure 4B, lanes 19 and 20) and degraded, underscoring a correlation between hyperphosphorylation and Fbw8-induced degradation; (3) the region spanning residues 522–574, which bears S527, is critical for proteolysis; (4) S636/S639 appeared not to be crucial for degradation; and (5) S307, S312, and S527, collectively, may mediate partial instability of IRS-1.

Of note, human IRS-1 (1–574) is devoid of major tyrosine phosphorylation sites for docking PI3-K (Y612, Y632, Y662, and Y732) (Shah and Hunter, 2005). Yet this fragment appeared in extensively phosphorylated forms (Figure 4B, lane 19) and was capable of Fbw8-induced degradation in HEK293 cells (Figure 4B, lane 14). Thus, it seems that at least in some cell types, the mTOR/S6K-catalyzed serine phosphorylation, and hence the degradation, of IRS-1, can be uncoupled from the receptor-mediated tyrosine phosphorylation, possibly due to high levels of mTOR/S6K in these cells. Consistent with this view, it was shown that a fragment of murine IRS-1, spanning amino acids 108–516, was phosphorylated by S6K in vitro (Harrington et al., 2004).

In Vitro Reconstitution of IRS-1 Ubiquitination by the CUL7 E3 Ligase

To determine whether the CUL7 E3 ligase supported the ubiquitination of IRS-1 in vitro, we employed insect-cell-produced human IRS-1 as a potential substrate and first evaluated its phosphorylation status by treatment with phosphatase or purified S6K. As revealed by immunoblot analysis, while incubation with either bacterial alkaline phosphatase or λ-phosphatase increased gel mobility of human IRS-1 markedly (Figure 5A, lanes 3 and 5), treatment with purified S6K accumulated the Ser307-phosphorylated form of IRS-1 (Figure 5B, lanes 3 and 4). These results suggest that while the insect-cell-produced human IRS-1 was phosphorylated extensively, Ser307, a well-characterized site for S6K (Harrington et al., 2004; Shah and Hunter, 2006), may be underphosphorylated.

To determine whether Fbw8 bound IRS-1 in vitro in a Ser307-phosphorylation-dependent manner, IRS-1, pretreated with or without S6K, was mixed with GST-Fbw8-Skp1 (shown in Figure S2A) immobilized to glutathione beads. As shown (Figure 5C, lane 4), GST-Fbw8-Skp1 interacted efficiently with IRS-1 only when treated with S6K. Omission of S6K (lanes 2 and 3) or substitution of GST-Fbw8-Skp1 with GST (lanes 3 and 5) largely abolished the interaction, demonstrating both the specificity of, and S6K phosphorylation dependency for, this binding reaction. However, because the IRS-1 preparation used was in extensively phosphorylated form (Figure 5A), it was unclear whether additional phosphorylation was required for the interaction between IRS-1 and Fbw8. In further support of the in vitro IRS-1-Fbw8 interaction, rabbit reticulolysate-synthesized IRS-1 was found to bind to GST-Fbw8/Skp1 as well (Figure S3).

To reconstitute ubiquitination in vitro, IRS-1 was preincubated with S6K, and affinity-purified CUL7 E3 (shown in Figure S2B) was then added to allow the assembly of the substrate-E3 complex. Ubiquitination was initiated by the addition of Ub, E1, and Ubc5c as the E2-conjugating enzyme, and reaction products were analyzed by immunoblot using anti-IRS-1 antibodies. As shown in Figure 5D, high molecular weight IRS-1 species were formed with all components present (lane 2). Removal of IRS-1 (lane 1), the CUL7 E3 (lane 3), Ubc5c (lane 4), or Ub (lane 5) abolished, or markedly inhibited, the reaction, indicating that these high molecular weight IRS-1 forms were the products of polyubiquitination reaction catalyzed by the CUL7 E3 and Ubc5c. Furthermore, as revealed by the kinetic experiment, efficient ubiquitination was detected 15 min after incubation (Figure 5E, lane 3), at which time point no significant ubiquitination was observed in the reaction lacking the CUL7 E3 (lane 6; see bottom graph for quantitative comparison). Taken together, the above results established that (1) phosphorylation of IRS-1 by S6K stimulated its interaction with Fbw8 and (2) the CUL7 E3 ligase was capable of catalyzing the polyubiquitination of IRS-1 in vitro, thus supporting a premise that the CUL7 E3 targets IRS-1 directly.

Inactivation of Fbw8 or CUL7 Accumulates IRS-1

To further establish IRS-1 as a substrate of the CUL7 E3, we sought to determine whether inactivation of Fbw8 or CUL7 would accumulate IRS-1. First, we employed siRNA to deplete Fbw8 and confirmed the depletion efficiency by using FF8HEK cell line, which constitutively expresses Flag-Fbw8 (Figure 6A). (The poor quality of anti-Fbw8 antibodies precluded the assessment of endogenous Fbw8.) When MCF-7 cells were treated with the same anti-Fbw8 siRNA, a marked increase in the level of IRS-1 was observed (Figure 6B, lanes 2 and 4).

To evaluate the effects of CUL7 inactivation, we analyzed embryonic fibroblasts derived from *Cul7*$^{-/-}$ mice, which were generated as described in the Supplemental Data (Figures S4 and S5). Immunoblot analysis confirmed the absence of CUL7 expression in the *Cul7*$^{-/-}$ MEFs (Figure S5C). Remarkably, the *Cul7*$^{-/-}$ MEFs accumulated IRS-1 to levels up to 5-fold higher than those observed in normal cells (Figure 6C, compare lanes 1 and 3). In the *Cul7*$^{+/+}$ MEFs,

treatment with IGF-1 for 30 min stimulated phosphorylation of IRS-1, as judged by the appearance of IRS-1 forms with decreased mobility (Figure 6C, lanes 1 and 2). In this setting, IRS-1 in *Cul7*$^{-/-}$ MEFs remained at high levels as well (Figure 6C, lanes 3 and 4). In addition, quantitative RT-PCR analysis revealed no significant difference in IRS-1 mRNA levels between *Cul7*$^{+/+}$ and *Cul7*$^{-/-}$ MEFs (Figure 6D). Taken together, the above findings demonstrate that IRS-1 is accumulated in cells deficient or devoid of the CUL7 E3 activity, thus agreeing strongly with the hypothesis that IRS-1 is the substrate of the CUL7 E3 ligase.

Loss of CUL7 Induces Senescence

IRS-1 mediates insulin/IGF-1 signaling by docking a set of key SH2-containing signaling proteins that include PI3-K, Grb2, Nck, and SHP2, thus activating the downstream Akt (via PI3-K) and RAS/MEK/ERK (through Grb2/SOS) pathways (Dearth et al., 2007). To compare the response by *CUL7*$^{-/-}$ and normal MEFs in IGF-1 signaling, extracts derived from cells treated with IGF-1 for varying time points were analyzed by immunoblots. The results revealed that *CUL7*$^{-/-}$ MEFs (1) maintained high levels of IRS-1 during the course of IGF-1 treatment and formed slow-migrating species (an indicative of hyperphosphorylated forms) after 30 min of IGF-1 exposure similarly as in the wild-type cells (Figure 6E, lanes 4–6 and 10–12); (2) exhibited 2-fold increase in the formation of active Akt (Akt^{pS473}) at the early time points following the treatment (7.5 and 15 min) in comparison to the normal MEFs (Figure 6F, graph); and (3) displayed sustained ERK/MEK activation, which was reflected by both magnitude and duration (Figure 6G, compare lanes 1–6 and lanes 7–12; graph). Of note, *CUL7*$^{-/-}$ MEFs contained activated Akt (Akt^{pS473}) and ERK (ERK$^{pT202/pY204}$) at levels higher than those observed in the wild-type cells in the absence of IGF-1 treatment (Figure S6A), suggesting a constitutive activation of these pathways. In addition, formation of ERK$^{pT202/pY204}$ in the *CUL7*$^{-/-}$ MEFs was inhibited by U0126, which blocks the activity of MEK (Figure S6B, compare lanes 4 and 10), but not by LY294002 (PI3-K inhibitor, compare lanes 4 and 6). The partial inhibition of ERK activation by PD98059 (Figure S6B, compare lanes 4 and 8) is likely due to the presence of elevated levels of the active form of MEK (MEK$^{pS217/221}$) in the *CUL7*$^{-/-}$ MEFs (Figure S6C, compare lanes 1 and 2). As previously demonstrated, PD98059 does not inhibit the activity of MEK$^{pS217/221}$ (Alessi et al., 1995). Finally, silencing IRS-1 in *CUL7*$^{-/-}$ MEFs by RNAi reduced formation of the active form of Akt (Akt^{pS473}) and ERK (ERK$^{pT202/pY204}$), most notably at the early time points after IGF-1 stimulation (Figure S7). These findings are consistent with the hypothesis that increased levels of IRS-1 in the *CUL7*$^{-/-}$ MEFs contribute to enhanced activation of Akt and ERK, observed in the presence and absence of IGF-1 treatment (Figures 6E–6G and Figure S6A). In agreement with these results, it was observed that overexpression of HA-Rheb and Myc-Fbw8 reduced IRS-1 by 50% in MCF-7 cells, exhibiting a delayed response to IGF-1 for the production of Ser^{473}-phosphorylated Akt (Figure S8, compare lanes 2 and 3 with lanes 5 and 6).

Of note, Tsutsumi et al. (2008) have reported upregulation of Insulin-like growth factor binding protein 1 and 2 (IGFBPs) in Fbw8 and CUL7 knockouts with subsequent hypophosphorylation of the IGF-1 receptor upon stimulation. Intriguingly, previous studies have shown that both PI3-K/Akt and MEK/ERK are capable of upregulating the expression of IGFBP2 and IGFBP1 (Mehrian-Shai et al., 2007; Frost et al., 2000), respectively. It is thus conceivable that enhanced PI3-K/Akt and ERK, due to the accumulation of IRS-1 in the *CUL7*$^{-/-}$ MEFs, may contribute to upregulation of IGFBPs.

However, Arai et al. (2003) have shown that *CUL7*$^{-/-}$ MEFs grew poorly. Confirming this finding, we observed that, at passage 2 and 6, the *CUL7*$^{-/-}$ MEFs exhibited a growth rate about 50% and 10%, respectively, of that seen with the normal cells (data not shown), suggesting a rapid decrease in growth capability of the *CUL7*$^{-/-}$ MEFs in culture with time. In addition, flow cytometry analysis revealed that *CUL7*$^{-/-}$ MEFs had a high G_1 but low S phase population

(Figure 7A), indicating that the *CUL7*$^{-/-}$ MEFs are predominantly arrested in G_1. Finally, an elevation of p16 and hypophosphorylated pRb was observed in the *CUL7*$^{-/-}$ MEFs (Figure 7B). Of note, we have also observed accumulation of p27 and p21 in the *CUL7*$^{-/-}$ MEFs, especially in the late cell passages (data not shown). In all, these findings suggest that the *CUL7*$^{-/-}$ MEFs are growth retarded and predominantly arrested in G_1, correlated with increased expression of p16/p27/p21 and hypophosphorylated pRb.

We evaluated whether *CUL7*$^{-/-}$ MEFs were senescent by staining for senescence-associated β-galactosidase activity (SA-β-gal) (Serrano et al., 1997). The percentage of SA-β-gal-positive cells in *CUL7*$^{-/-}$ MEFs was high (>40%) and increased over passage in culture, reaching >60% (Figure 7C). In contrast, no more than 8% of the *CUL7*$^{+/+}$ MEFs were SA-β-gal-positive (Figure 7C). Moreover, *CUL7*$^{-/-}$ MEFs exhibited flat and enlarged morphology (Figure 7D), characteristic of senescent cells (Mooi and Peeper, 2006). Thus, *CUL7*$^{-/-}$ MEFs possessed a number of phenotypic features associated with oncogene-induced senescence: sustained activation of MAPK and increased Akt activity, cell-cycle arrest, induction of p16/pRb, enhanced SA-β-gal-activity, and flat and enlarged morphology.

DISCUSSION

Role of CUL7 E3-Mediated Degradation of IRS-1 in mTOR-Triggered Negative-Feedback Loop

Haruta et al. (2000) first observed the proteolytic turnover of IRS-1 during prolonged exposure to insulin, a process that requires PI3-K and mTOR. In addition, the integrity of amino acid residue Ser12, a target of mTOR, was shown to mediate, at least in part, the degradation of human IRS-1 (Greene et al., 2003). Previous studies have also implicated a role for the SOCS-containing E3 ligases in IRS-1 degradation (Rui et al., 2002). Despite these advances, however, the cellular mechanisms by which IRS-1 is targeted for degradation by an E3(s) in an mTOR-dependent manner remained elusive.

Our study identified IRS-1 as a proteolytic target of the CUL7 E3 ligase and revealed a directing role for mTOR/S6K phosphorylation in this degradation process. Fbw8, the substrate-targeting subunit of the CUL7 E3 ligase, was shown to interact with IRS-1 in vivo (Figure 1) and in vitro (Figure 5C; Figure S3). This interaction likely requires phosphorylation of IRS-1 by mTOR/S6K, because phosphorylation of IRS-1 by S6K at Ser307 stimulated its interaction with Fbw8 in vitro (Figure 5C) and the S307/S312/S527/S636/S639 quintuple alanine substitution mutation diminished the ability of IRS-1 to interact with Fbw8 in vivo (Figure S1B). Second, overexpression of Fbw8 and CUL7 in different cell types markedly reduced the steady-state level of IRS-1 and shortened its half-life (Figure 2). The evidence for the requirement of mTOR/S6K in this degradation includes the following: (1) treatment with rapamycin inhibited the Fbw8-mediated degradation of IRS-1 (Figure 3A), (2) overexpression of Rheb stimulated the proteolysis (Figure 3B), and (3) elimination of several mTOR/S6K target sites within human IRS-1 yielded a partial resistance to degradation by Fbw8 (Figure 4A). Third, using in vitro reconstitution, it was observed that the CUL7 E3 ligase was capable of catalyzing the polyubiquitination of IRS-1 (Figures 5D and 5E). Lastly, IRS-1 accumulated in cells depleted of Fbw8 by RNA interference and in mouse embryonic fibroblasts deleted of *Cul7* (Figures 6B and 6C).

On the basis of the above findings, we propose that targeted degradation of IRS-1 by the CUL7 E3 ligase constitutes a core component of the mTOR negative-feedback loop. This E3 recognizes IRS-1 in seryl-phosphorylated forms generated by mTOR/S6K and mediates its polyubiquitination and eventual proteasomal destruction (Figure 3C). The mTOR/IRS-1 negative-feedback loop is thought to restrain the activity of PI3-K, whose aberrant activation is a significant contributing factor to cancer initiation and progression. It was shown that

circumventing the IRS-1 negative-feedback loop results in enhanced Akt activation as well as more frequent and aggressive hemangiomas (Manning et al., 2005).

The IRS-1 Degron: Organization and Activation

The nature of the IRS-1 degradation signal (degron) appears to be complex. Combined site-directed mutagenesis and deletion studies suggest that the IRS-1 degron is located at the N-terminal half of the protein, with the C-terminal boundary around amino acid residue 574 (Figure 4B), and that it may feature multiple mTOR/S6K serine residues including S307, S312, and S527 because of their role in mediating partial levels of IRS-1 instability (Figure 4A). In vitro, Ser307 phosphorylation by S6K enhanced the ability of IRS-1 to interact with the Fbw8-Skp1 complex (Figure 5C). These findings point to a possibility that IRS-1 may contain multiple degron motifs. It is well known that HIF-1α contains a degron/ODD of approximately 200 amino acids that confers oxygen-dependent degradation. The HIF-1α ODD is composed of two separate prolyl hydroxylation motifs capable of interacting with the pVHL E3 ligase (Masson et al., 2001). It was shown that both prolyl hydroxylation motifs were able to mediate partial levels of HIF-1α instability (Masson et al., 2001).

IRS-1 may employ multiple phosphodegron segments, each with suboptimal affinity for Fbw8. In this scenario, full activation of the IRS-1 degron may require a high threshold of mTOR/S6K activities, which sets this signaling mediator for polyubiquitination and degradation. Alternatively, IRS-1 may possess a single phosphodegron, which could be phosphorylated only after other serine sites, located outside of the degron, had acquired phosphates through the action of mTOR/S6K. This hierarchical order of phosphorylation events has been observed with Cdc25A, where phosphorylation at S76 is a “priming step” required for the phosphorylation of S82 within the “DSG” degron motif, which triggers its interaction with $SCF^{\beta TrCP}$ for ubiquitination (Donzelli et al., 2004). This scenario might also set a phosphorylation threshold that requires high levels of mTOR/S6K for IRS-1 degradation. Whatever the case, the requirement of multiserine phosphorylation for the degradation of IRS-1 may reflect a biological need to fine-tune PI3-K signaling in accordance with the magnitude and duration of the mTOR/S6K activity.

Role of CUL7 in Senescence

Oncogene-induced senescence is an antiproliferative program characterized by sequential activation of two opposing, growth-regulating activities. Initially, there must be an oncogenic activation that renders cells hyperproliferative. In response, tumor suppressor activities, mediated by p53 and/or pRB, are turned on to drive these cells into a terminally arrested state (reviewed in Campisi, 2005; Mooi and Peeper, 2006). Given the robust accumulation of IRS-1 and the associated senescence phenotype observed in the *CUL7*$^{-/-}$ MEFs (Figure 6 and Figure 7), our working hypothesis is that aberrant accumulation of IRS-1, resulting from inactivation of the CUL7 E3, is the “oncogenic stimulus” that triggers the onset of cellular senescence, presumably through sustained MAPK activation and/or increased Akt signaling (Figure 6), both of which were previously shown to induce senescence (Campisi, 2005; Mooi and Peeper, 2006). In addition, a previous study by Maier et al. (2004) showed that activated IGF-1 signaling, induced by overexpression of the p53 isoform p44, yielded sustained ERK activation, p21 induction, and senescence. However, the current study does not rule out the possibility that accumulation of an additional unknown substrate(s) of the CUL7 E3 ligase may contribute to the senescence phenotype associated with the *CUL7*$^{-/-}$ MEFs. A recent study by Sarkisian et al. (2007) revealed that the majority of Ras-induced senescent cells do not re-enter the cell cycle after downregulation of the oncogenic trigger in vivo, suggesting that the oncogenic activator, while responsible for initiating senescence, may not be required to maintain senescent states. In this regard, IRS-1 was found dispensable for senescence maintenance as RNAi-mediated depletion of IRS-1 was unable to reverse senescence in

CUL7$^{-/-}$ MEFs (data not shown). It is hoped that continuing investigation will produce nondegradable forms of IRS-1, which would allow us to determine whether such mutants could generate high levels of PI3-K/Akt and RAS/MAPK activities that exert constitutive oncogenic stress, leading to senescence response.

IRS-1 is a critical component that mediates insulin/IGF-1 signaling and hence plays an important role in organismal growth and aging. Dysregulation of IRS-1 has been implicated in the pathogenesis of type II diabetes and cancer. Results presented in this study demonstrate a pivotal role for the CUL7 E3 ligase in targeting IRS-1 for Ub-dependent degradation and thus potentially provide new avenues in altering IRS-1 function in a manner that would advance our interest in treatment of human disease. In this context, it is of particular interest to note that this study has uncovered a regulatory function for CUL7 in the onset of cellular senescence, raising hypotheses of whether the CUL7 E3 substrates that include IRS-1, when aberrantly accumulated, may act as an "oncogenic trigger(s)" for senescence and whether senescence is a contributing factor for the pathogenesis of growth retardation observed in patients with 3-M and Yakuts dwarfism syndromes.

EXPERIMENTAL PROCEDURES

Reagents

Preparation of plasmids for expression of human IRS-1, truncations, and point mutants, and for assembly of the bacterially expressed GST-Fbw8/Skp1 complex, is described in detail in the Supplemental Data. Plasmids for Flag-CUL7 and Myc-Fbw8 were as described previously (Dias et al., 2002). HA-Rheb was a gift from Kunliang Guan (University of Michigan). Generation of anti-Fbw8 antibody, and sources for other antibodies as well as ubiquitination reagents used in this study, are described in the Supplemental Data.

Cells

Cul7$^{-/-}$ mouse embryonic fibroblasts (MEFs) were described in detail in the Supplemental Data (Figures S4 and S5). HEK293 and MCF-7 cells were grown in Dulbecco's modified Eagle medium supplemented with 10% fetal bovine serum (GIBCO). FF8HEK, a cell line derived from HEK293 and constitutively expressing Flag-Fbw8, was generated by using a procedure as described previously (Dias et al., 2002). For transfection, expression vectors were introduced into HEK293 or MCF-7 cells by using Lipofectamine 2000 (Invitrogen) according to the manufacturer's protocol. Procedures for cell lysis, immunoprecipitation, and RT-PCR are provided in the Supplemental Data.

CHX Chase Assay

MCF-7 cells were plated at a density of 10^6 per 6 cm diameter dish, allowed to adhere overnight, and then subjected to transfection as described previously. At 42 hr posttransfection, cells were treated with CHX (Sigma) at a final concentration of 25 μg/ml and were harvested at the indicated time.

In Vitro Ubiquitination

Purified human IRS-1 (0.4 pmol) was incubated with S6K (0.01 ng) at 37°C for 15 min in a reaction mixture (20 μl) containing 50 mM Tris-HCl (pH 7.4), 5 mM $MgCl_2$, 0.5 mM DTT, 2 mM ATP, 0.1 mg/ml BSA, 2 mM NaF, and 10 nM okadaic acid. Affinity-purified CUL7 E3 (~0.5 pmol; shown in Figure S2B) was added and the mixture was incubated at room temperature for 5 min. Finally, ubiquitination agents (28 μM PK-Ub, 2 nM E1, and 2 μM Ubc5c) were added, and the final reaction volume was adjusted to 30 μl. Incubation continued

at 37°C for 60 min or times as specified. The reaction products, separated by 4%–20% SDS-PAGE, were analyzed by immunoblot analysis using anti-IRS-1 antibody.

Supplementary Material

Refer to Web version on PubMed Central for supplementary material.

ACKNOWLEDGMENTS

We thank K. Bass, W. Zhang, S. Das, P. Hamard, L. Carvajal, B. Zhao, X. Wang, A. Chan, L.-H. Wang, S. Aaronson, and S. Muehlich for technical assistance and K. Guan for the Rheb plasmid. A.S. was supported by a research fellowship from the German Research Foundation. This study was supported by National Institutes of Health grants HL075609 (L.J.F.), CA88325 and resource grant RR17802 (R.W.), and CA095634 and GM61051 (Z.-Q.P.).

REFERENCES

Alessi DR, Cuenda A, Cohen P, Dudley DT, Saltiel AR. PD 098059 is a specific inhibitor of the activation of mitogen-activated protein kinase kinase in vitro and in vivo. J. Biol. Chem 1995;270:27489–27494. [PubMed: 7499206]

Andrews P, He YJ, Xiong Y. Cytoplasmic localized ubiquitin ligase cullin 7 binds to p53 and promotes cell growth by antagonizing p53 function. Oncogene 2006;25:4534–4548. [PubMed: 16547496]

Arai T, Kasper JS, Skaar JR, Ali SH, Takahashi C, DeCaprio JA. Targeted disruption of p185/Cul7 gene results in abnormal vascular morphogenesis. Proc. Natl. Acad. Sci. USA 2003;100:9855–9860. [PubMed: 12904573]

Campisi J. Senescent cells, tumor suppression, and organismal aging: good citizens, bad neighbors. Cell 2005;120:513–522. [PubMed: 15734683]

Daud AI, Lanson NA Jr, Claycomb WC, Field LJ. Identification of SV40 large T-antigen-associated proteins in cardiomyocytes from transgenic mice. Am. J. Physiol 1993;264:H1693–H1700. [PubMed: 8498581]

Dearth RK, Cui X, Kim HJ, Hadsell DL, Lee AV. Oncogenic transformation by the signaling adaptor proteins insulin receptor substrate (IRS)-1 and IRS-2. Cell Cycle 2007;6:705–713. [PubMed: 17374994]

Dias DC, Dolios G, Wang R, Pan ZQ. CUL7: a DOC domain-containing cullin selectively binds Skp1.Fbx29 to form an SCF-like complex. Proc. Natl. Acad. Sci. USA 2002;99:16601–16606. [PubMed: 12481031]

Donzelli M, Busino L, Chiesa M, Ganoth D, Hershko A, Draetta GF. Hierarchical order of phosphorylation events commits Cdc25A to betaTrCP-dependent degradation. Cell Cycle 2004;3:469–471. [PubMed: 14752276]

Dowell JD, Tsai SC, Dias-Santagata DC, Nakajima H, Wang Z, Zhu W, Field LJ. Expression of a mutant p193/CUL7 molecule confers resistance to MG132- and etoposide-induced apoptosis independent of p53 or Parc binding. Biochim. Biophys. Acta 2007;1773:358–366. [PubMed: 17229476]

Frost RA, Nystrom GJ, Lang CH. Stimulation of insulin-like growth factor binding protein-1 synthesis by interleukin-1beta: requirement of the mitogen-activated protein kinase pathway. Endocrinology 2000;141:3156–3164. [PubMed: 10965886]

Greene MW, Sakaue H, Wang L, Alessi DR, Roth RA. Modulation of insulin-stimulated degradation of human insulin receptor substrate-1 by serine 312 phosphorylation. J. Biol. Chem 2003;278:8199–8211. [PubMed: 12510059]

Harrington LS, Findlay GM, Gray A, Tolkacheva T, Wigfield S, Rebholz H, Barnett J, Leslie NR, Cheng S, Shepherd PR, et al. The TSC1-2 tumor suppressor controls insulin-PI3-K signaling via regulation of IRS proteins. J. Cell Biol 2004;166:213–223. [PubMed: 15249583]

Harrington LS, Findlay GM, Lamb RF. Restraining PI3-K: mTOR signaling goes back to the membrane. Trends Biochem. Sci 2005;30:35–42. [PubMed: 15653324]

Haruta T, Uno T, Kawahara J, Takano A, Egawa K, Sharma PM, Olefsky JM, Kobayashi M. A rapamycin-sensitive pathway down-regulates insulin signaling via phosphorylation and proteasomal degradation of insulin receptor substrate-1. Mol. Endocrinol 2000;14:783–794. [PubMed: 10847581]

Hershko A, Ciechanover A. The ubiquitin system. Annu. Rev. Biochem 1998;67:425–479. [PubMed: 9759494]

Huber C, Dias-Santagata D, Glaser A, O'Sullivan J, Brauner R, Wu K, Pearce K, Wang R, Luisa M, Uzielli G, et al. Identification of CUL7 mutations in the 3-M syndrome. Nat. Genet 2005;37:1119–1124. [PubMed: 16142236]

Jung P, Verdoodt B, Bailey A, Yates JR 3rd, Menssen A, Hermeking H. Induction of Cullin 7 by DNA damage attenuates p53 function. Proc. Natl. Acad. Sci. USA 2007;104:11388–11393. [PubMed: 17586686]

Kasper JS, Kuwabara H, Arai T, Ali SH, DeCaprio JA. Simian virus 40 large T antigen's association with the CUL7 SCF complex contributes to cellular transformation. J. Virol 2005;79:11685–11692. [PubMed: 16140746]

Kaustov L, Lukin J, Lemak A, Duan S, Ho M, Doherty R, Penn LZ, Arrowsmith CH. The conserved CPH domains of Cul7 and PARC are protein-protein interaction modules that bind the tetramerization domain of p53. J. Biol. Chem 2007;282:11300–11307. [PubMed: 17298945]

Kim SS, Shago M, Kaustov L, Boutros PC, Clendening JW, Sheng Y, Trentin GA, Barsyte-Lovejoy D, Mao DY, Kay R, et al. CUL7 is a novel antiapoptotic oncogene. Cancer Res 2007;67:9616–9622. [PubMed: 17942889]

Kohrman DC, Imperiale MJ. Simian virus 40 large T antigen stably complexes with a 185-kilodalton host protein. J. Virol 1992;66:1752–1760. [PubMed: 1310776]

Maier B, Gluba W, Bernier B, Turner T, Mohammad K, Guise T, Sutherland A, Thorner M, Scrable H. Modulation of mammalian life span by the short isoform of p53. Genes Dev 2004;18:306–319. [PubMed: 14871929]

Maksimova N, Hara K, Miyashita A, Nikolaeva I, Shiga A, Nogovicina A, Sukhomyasova A, Argunov V, Shvedova A, Ikeuchi T, et al. Clinical, molecular and histopathological features of short stature syndrome with novel CUL7 mutation in Yakuts: new population isolate in Asia. J. Med. Genet 2007;44:772–778. [PubMed: 17675530]

Manning BD, Logsdon MN, Lipovsky AI, Abbott D, Kwiatkowski DJ, Cantley LC. Feedback inhibition of Akt signaling limits the growth of tumors lacking Tsc2. Genes Dev 2005;19:1773–1778. [PubMed: 16027169]

Masson N, Willam C, Maxwell PH, Pugh CW, Ratcliffe PJ. Independent function of two destruction domains in hypoxia-inducible factor-alpha chains activated by prolyl hydroxylation. EMBO J 2001;20:5197–5206. [PubMed: 11566883]

Mehrian-Shai R, Chen CD, Shi T, Horvath S, Nelson SF, Reichardt JK, Sawyers CL. Insulin growth factor-binding protein 2 is a candidate biomarker for PTEN status and PI3K/Akt pathway activation in glioblastoma and prostate cancer. Proc. Natl. Acad. Sci. USA 2007;104:5563–5568. [PubMed: 17372210]

Mooi WJ, Peeper DS. Oncogene-induced cell senescence-halting on the road to cancer. N. Engl. J. Med 2006;355:1037–1046. [PubMed: 16957149]

Okabe H, Lee SH, Phuchareon J, Albertson DG, McCormick F, Tetsu O. A critical role for FBXW8 and MAPK in cyclin D1 degradation and cancer cell proliferation. PLoS ONE 2006;1:e128. [PubMed: 17205132]

Petroski MD, Deshaies RJ. Function and regulation of cullin-RING ubiquitin ligases. Nat. Rev. Mol. Cell Biol 2005;6:9–20. [PubMed: 15688063]

Rui L, Yuan M, Frantz D, Shoelson S, White MF. SOCS-1 and SOCS-3 block insulin signaling by ubiquitin-mediated degradation of IRS1 and IRS2. J. Biol. Chem 2002;277:42394–42398. [PubMed: 12228220]

Sarkisian CJ, Keister BA, Stairs DB, Boxer RB, Moody SE, Chodosh LA. Dose dependent oncogene-induced senescence in vivo and its evasion during mammary tumorigenesis. Nat. Cell Biol 2007;9:493–505. [PubMed: 17450133]

Serrano M, Lin AW, McCurrach ME, Beach D, Lowe SW. Oncogenic ras provokes premature cell senescence associated with accumulation of p53 and p16INK4a. Cell 1997;88:593–602. [PubMed: 9054499]

Shah OJ, Hunter T. Tuberous sclerosis and insulin resistance: unlikely bedfellows reveal a TORrid affair. Cell Cycle 2005;4:122–127.

Shah OJ, Hunter T. Turnover of the active fraction of IRS1 involves raptor-mTOR- and S6K1-dependent serine phosphorylation in cell culture models of tuberous sclerosis. Mol. Cell. Biol 2006;26:6425–6434. [PubMed: 16914728]

Shah OJ, Wang Z, Hunter T. Inappropriate activation of the TSC/Rheb/mTOR/S6K cassette induces IRS1/2 depletion, insulin resistance, and cell survival deficiencies. Curr. Biol 2004;14:1650–1656. [PubMed: 15380067]

Tsai SC, Pasumarthi KB, Pajak L, Franklin M, Patton B, Wang H, Henzel WJ, Stults JT, Field LJ. Simian virus 40 large T antigen binds a novel Bcl-2 homology domain 3-containing proapoptosis protein in the cytoplasm. J. Biol. Chem 2000;275:3239–3247. [PubMed: 10652310]

Tsunematsu R, Nishiyama M, Kotoshiba S, Saiga T, Kamura T, Nakayama KI. Fbxw8 is essential for Cul1-Cul7 complex formation and for placental development. Mol. Cell. Biol 2006;26:6157–6169. [PubMed: 16880526]

Tsutsumi T, Kuwabara H, Arai T, Xiao Y, Decaprio JA. Disruption of fbxw8 gene results in pre- and postnatal growth retardation in mice. Mol. Cell. Biol 2008;28:743–751. [PubMed: 17998335]

White MF. IRS proteins and the common path to diabetes. Am. J. Physiol. Endocrinol. Metab 2002;283:E413–E422. [PubMed: 12169433]

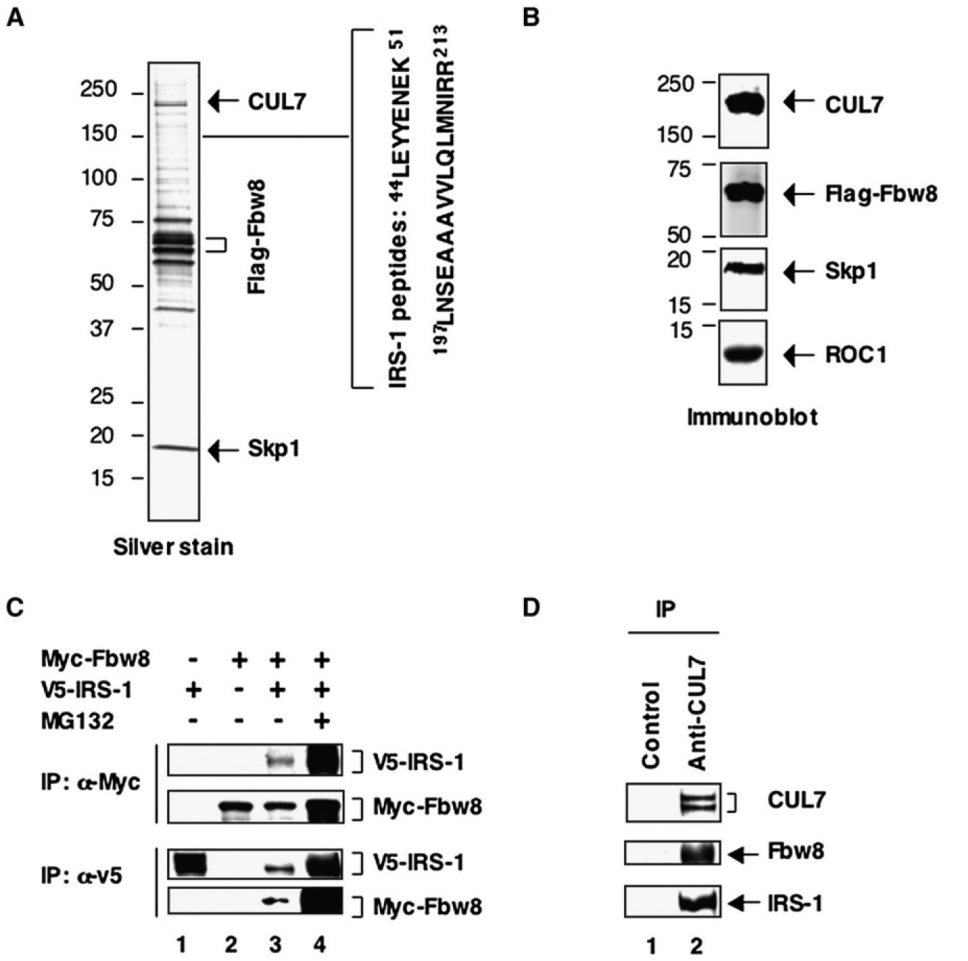

Figure 1. Analysis of Fbw8/IRS-1 Interaction In Vivo

(A and B) Analysis of the Flag-Fbw8 immunoprecipitates. Silver stain (A) and immunoblot (B) analysis of Flag-Fbw8-associated proteins, isolated as described in the Supplemental Data.

(C) Interactions between ectopically expressed Fbw8 and IRS-1. HEK293 cells were transfected with vectors expressing V5-IRS-1 and Myc-Fbw8. At 48 hr posttransfection, cells were harvested. Extracts (500 μg) were used for immunoprecipitation with anti-Myc or anti-V5 antibodies followed by separation through 6% SDS-PAGE and immunoblot analysis as indicated.

(D) Association between endogenous IRS-1 and CUL7. Extracts (1 mg of protein) from MCF-7 cells were subject to immunoprecipitation with IgG (lane 1) or anti-CUL7 (Mab38) antibodies (lane 2). The precipitates were separated by 6% SDS-PAGE followed by immunoblot analysis.

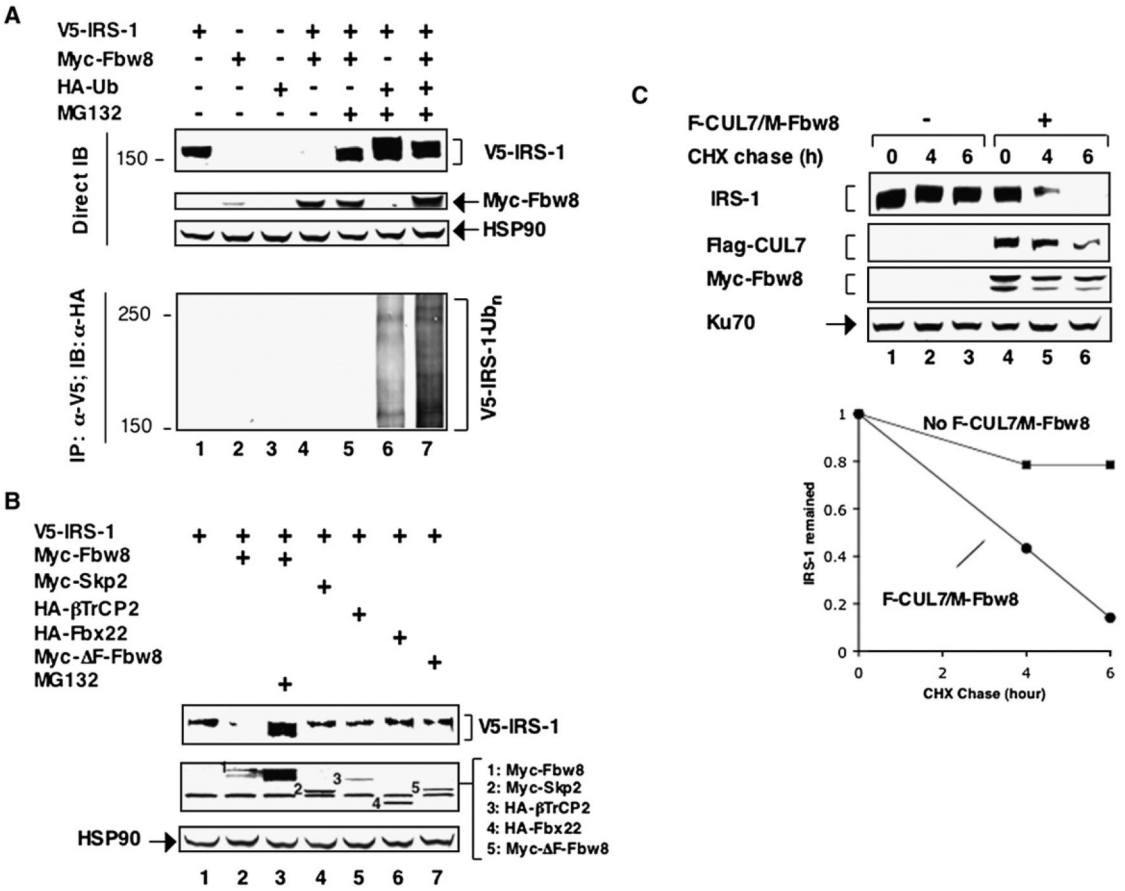

Figure 2. Fbw8 Promotes the Degradation of IRS-1

(A) Enhanced degradation of IRS-1 in HEK293 cells that overexpress Fbw8. HEK293 cells were cotransfected with vectors expressing V5-IRS-1, Myc-Fbw8, and HA-Ub, singly or in combination. At 42 hr posttransfection, where indicated, cells were treated with MG132 (10 μM) for 6 hr. Extracts (50 μg of protein) were subject to direct immunoblot analysis to monitor the changes in the level of V5-IRS-1 and to reveal the presence of Myc-Fbw8. Equal loading was verified by anti-HSP90 immunoblot. Note that the protein levels of β-actin (Figure 4B), HSP90, and Ku70 (Figure 2C and Figure 6A) were found unchanged in cells ectopically expressing Fbw8 and/or CUL7, and therefore each serves as an internal control for equal loading of samples in the immunoblot analysis described throughout the text. To reveal polyubiquitination, extracts (~1 mg of protein) from HEK293 cells were immunoprecipitated with anti-V5 antibodies. The precipitates were separated by 6% SDS-PAGE followed by immunoblot with anti-HA antibodies.

(B) The specificity of the Fbw8-induced degradation of IRS-1. HEK293 cells were cotransfected with vectors expressing V5-IRS-1, Myc-Fbw8, or other F box proteins as indicated and were analyzed as in (A). The expression of Myc-Fbw8 or other F box proteins was determined by sequential immunoblot analysis, first reacted with anti-Myc and then anti-HA antibodies, followed by visualization using the Odyssey Infrared Imaging System.

(C) CHX chase analysis. MCF-7 cells were transfected with pcDNA3.1 empty vectors (lanes 1–3) or vectors expressing Flag-CUL7 and Myc-Fbw8 (lanes 4–6). At 42 hr posttransfection, cells were treated with CHX (25 μg/ml) and chased for times as indicated. Extracts (50 μg) were separated by 6% SDS-PAGE followed by immunoblot analysis to monitor the levels of

endogenous IRS-1, and ectopically expressed Flag-CUL7 and Myc-Fbw8. The remaining IRS-1 was quantitated by the Odyssey Infrared Imaging System and expressed graphically.

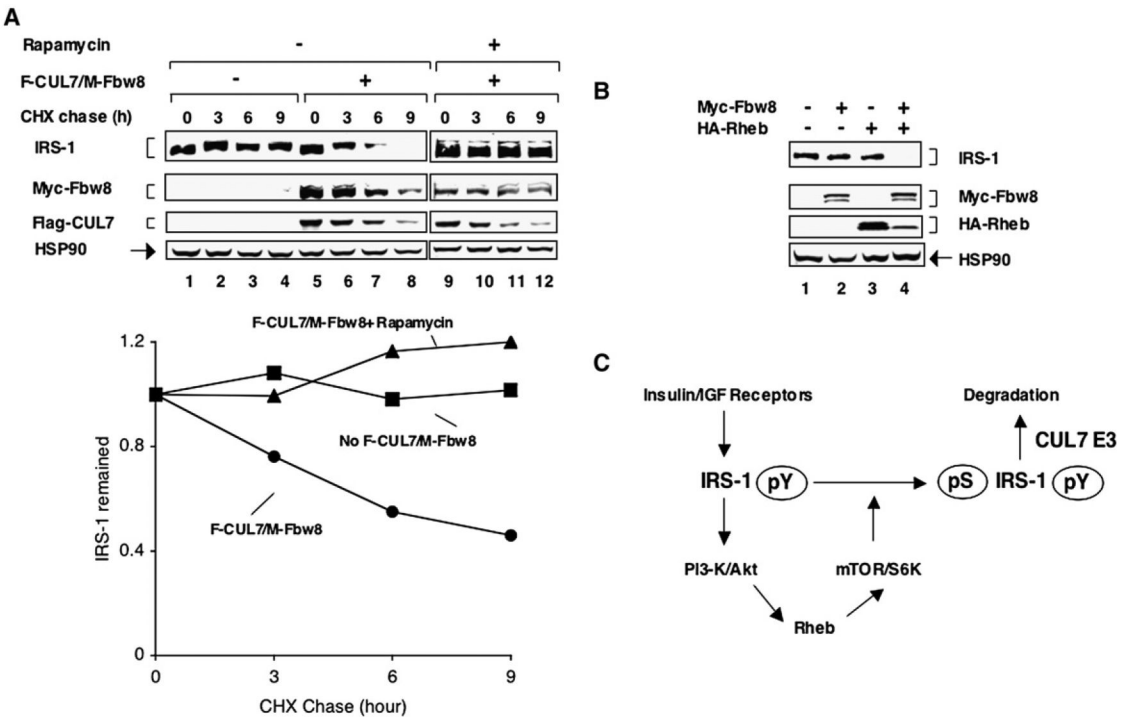

Figure 3. mTOR Is Required for the Degradation of IRS-1 by Fbw8

(A) CHX chase. MCF-7 cells were transfected with pcDNA3.1 empty vectors (lanes 1–4) or vectors expressing Flag-CUL7 and Myc-Fbw8 (lanes 5–12). At 24 hr posttransfection, cells were treated with (lanes 9–12) or without (lanes 1–8) rapamycin (100 nM). Twenty-four hours later, CHX (25 μg/ml) was added and chased for times as indicated, followed by immunoblot analysis as described in Figure 2C.

(B) Enhanced degradation of IRS-1 by Fbw8 and Rheb. MCF-7 cells were cotransfected with vectors expressing Myc-Fbw8 and HA-Rheb. At 48 hr posttransfection, cells were harvested and the extracts (50 μg of protein) were analyzed by immunoblot to monitor the changes in the level of endogenous IRS-1 and to reveal the presence of ectopically expressed proteins.

(C) A model for a role of the CUL7 E3 in the mTOR-IRS-1 negative-feedback regulation. Following insulin/IGF-1-mediated activation of receptors, IRS-1 becomes tyrosyl-phosphorylated and docks PI3-K, leading to activation of Akt and then Rheb, which turns on mTOR/S6K. The elevated mTOR/S6K serine-phosphorylate IRS-1, which sets the CUL7 E3-dependent ubiquitination and eventual degradation.

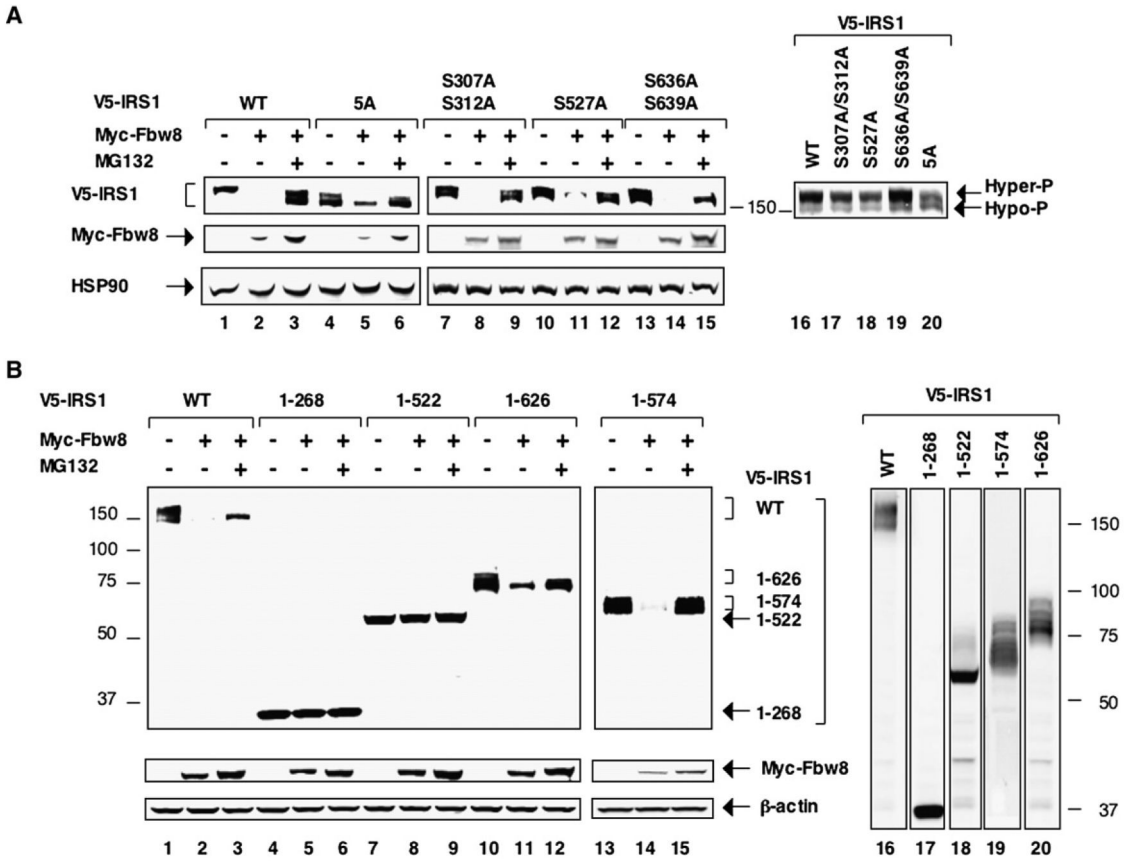

Figure 4. Analysis of IRS-1 Degradation Signals

(A) Elimination of phosphorylation at S307/S312/S527/S636/S639 renders V5-IRS-1 partially resistant to degradation by Fbw8. HEK293 cells were cotransfected with vectors expressing V5-IRS-1, Myc-Fbw8, or various point mutants as indicated and were analyzed as described in Figure 2A. 5A refers to a V5-IRS-1 quintuple mutant, replacing S307/S312/S527/S636/S639 with alanines. Of note, the wild-type V5-IRS-1 and variants V5-IRS-1$^{S307A/S312A}$, V5-IRS-1^{S527A}, and V5-IRS-1$^{S636A/S639A}$ appeared in hyperphosphorylated forms predominantly (lanes 16–19). In contrast, nearly half of V5-IRS-1^{5A} was present in hypophosphorylated species (lane 20), suggesting that the quintuple mutation significantly reduced hyperphosphorylation of IRS-1. These findings argued for a positive correlation between IRS-1 hyperphosphorylation and Fbw8-imposed degradation.

(B) Overexpression of Fbw8 induces the degradation of IRS-1 (1–574) and IRS-1 (1–626). HEK293 cells were cotransfected with vectors expressing Myc-Fbw8, V5-IRS-1 (amino acids 1–1242), or its truncated derivatives as indicated and were analyzed as described in Figure 2A.

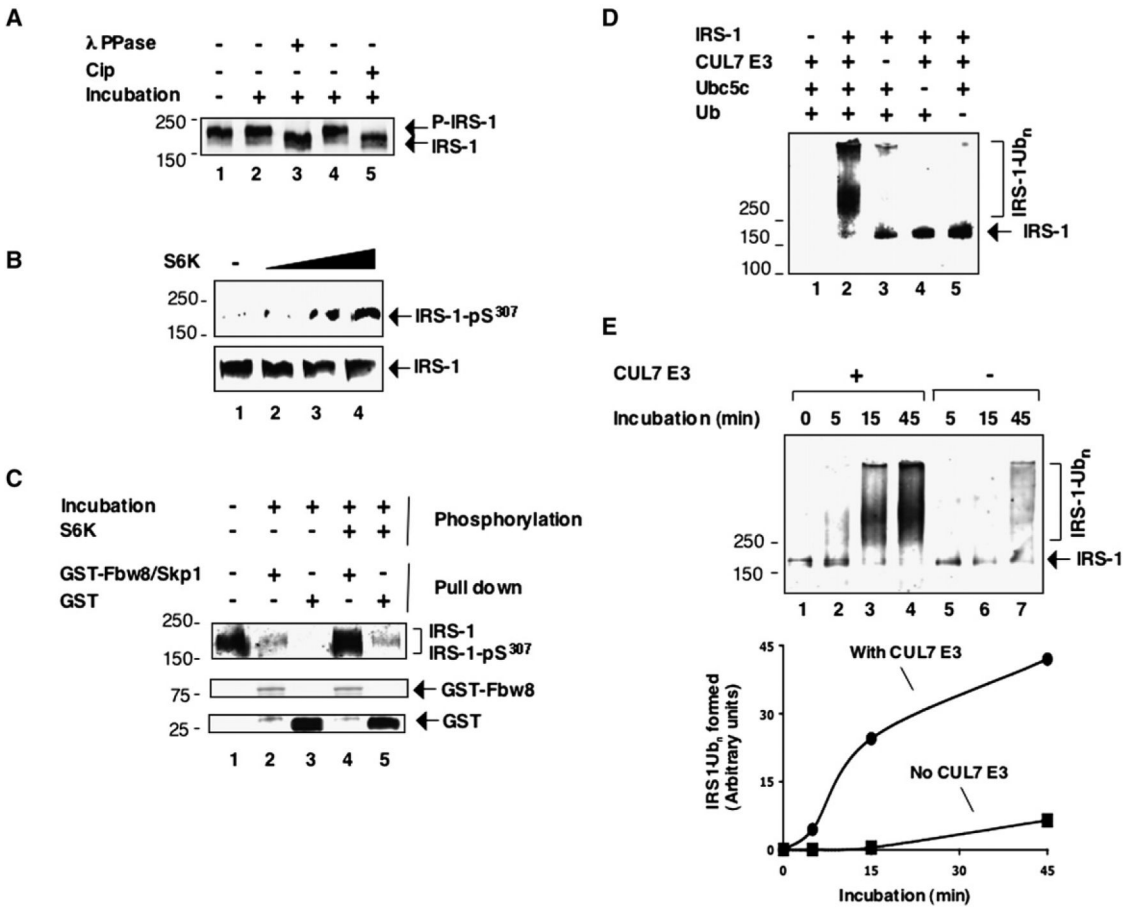

Figure 5. The CUL7 E3 Binds IRS-1 and Promotes Its Polyubiquitination In Vitro

(A) Dephosphorylation of IRS-1. Purified insect-cell-produced human IRS-1 (60 ng) was incubated with λ phosphatase (1 unit; lane 3) or alkaline phosphatase (1 unit; lane 5) at 37°C for 30 min. The reaction products were analyzed by immunoblot analysis using anti-IRS-1 antibody.

(B) Phosphorylation of IRS-1 by S6K. Purified human IRS-1 (60 ng) was incubated with S6K (0.1, 1, and 10 pg for lanes 2–4, respectively) at 37°C for 30 min. The reaction products were analyzed by immunoblot analysis using antibodies recognizing IRS-1 phosphorylated at Ser307 (upper) or for total IRS-1.

(C) In vitro interaction between Fbw8 and IRS-1. The binding experiment was carried out as described in the Supplemental Data, with input (20%) shown in lane 1.

(D and E) Reconstitution of in vitro polyubiquitination of IRS-1 by the CUL7 E3 and kinetic analysis. Polyubiquitination of IRS-1 was reconstituted as described in the Experimental Procedures.

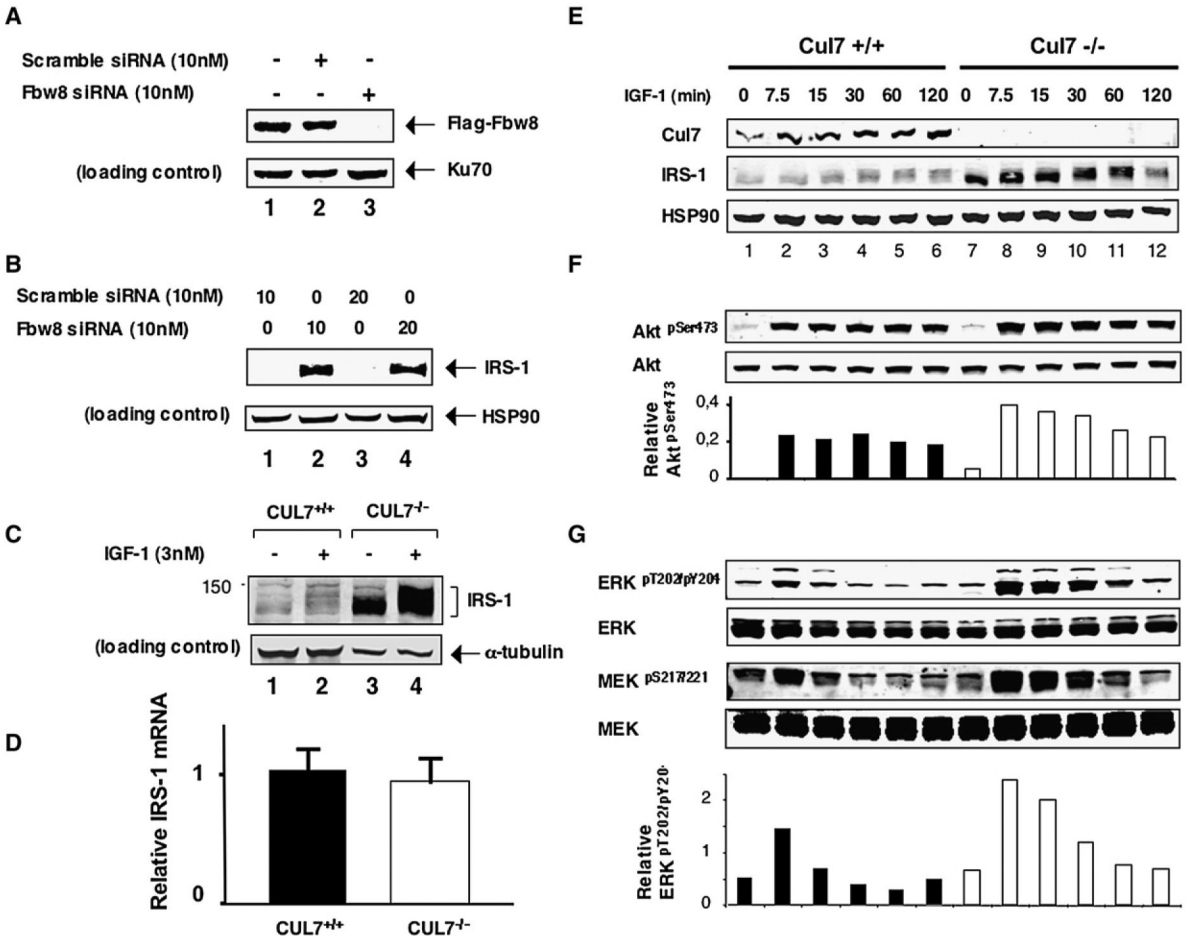

Figure 6. Inactivation of Fbw8 or CUL7 Accumulates IRS-1

(A) SiRNA-mediated depletion of Fbw8. FF8HEK cells, constitutively expressing Flag-Fbw8, were treated with scramble siRNA (lane 2) or Fbw8-siRNA (lane 3) at a concentration of 10 nM. SiRNA was obtained from Dharmacon, and transfection was carried out following manufacturers' instruction. At 48 hr posttransfection, cells were harvested. Extracts (50 μg) were separated by 6% SDS-PAGE followed by immunoblot analysis to monitor the levels of Flag-Fbw8.

(B) Fbw8 depletion accumulates IRS-1. MCF-7 cells were transfected with scramble or Fbw8 siRNA at indicated concentrations for 48 hr. Extracts (50 μg) were subject to immunoblot analysis to monitor the levels of endogenous IRS-1.

(C) Accumulation of IRS-1 in *Cul7*$^{-/-}$ MEFs. MEFs were serum-starved for 16 hr prior to treatment with (lanes 2 and 4) or without (lanes 1 and 3) IGF-1 (3 nM) for 30 min. Extracts (100 μg of protein) were separated by 6% SDS-PAGE followed by immunoblot analysis to monitor the levels of endogenous IRS-1.

(D) RT-PCR analysis of IRS-1 mRNA. IRS-1 mRNA from *CUL7*$^{+/+}$ or *CUL7*$^{-/-}$ MEFs was analyzed using a procedure described in the Supplemental Data. Note that the graph integrates the results of three independent experiments, with error bars for the calculated standard deviation.

(E–G) *CUL7*$^{-/-}$ MEFs accumulate IRS-1 and exhibit increased activation of Akt and MEK/ERK. MEFs derived from *CUL7*$^{+/+}$ (lanes 1–6) or *CUL7*$^{-/-}$ (lanes 7–12) were serum-starved for 16 hr prior to treatment with (lanes 2–6 and 8–12) or without (lanes 1 and 7) IGF-1 (3 nM)

for indicated times. Extracts (100 μg of protein) were separated by 4%–20% SDS-PAGE followed by immunoblot analysis to monitor the levels of CUL7, IRS-1, phosphorylated Akt, MEK, and ERK, as well as HSP90 (as a control for equal loading; note that *CUL7*$^{+/+}$ and *CUL7*$^{-/-}$ MEFs contain identical levels of α-actinin, HSP90, or tubulin [Figure S6D]). The relative ratio of phosphorylated Atk (or ERK) versus total pool is quantitated and shown graphically. Note that in Figure 6E, lane 12, there was a reduction of IRS-1 at 120 min after IGF-1 treatment. This decrease, however, was not reproducible and is most likely an experimental variation.

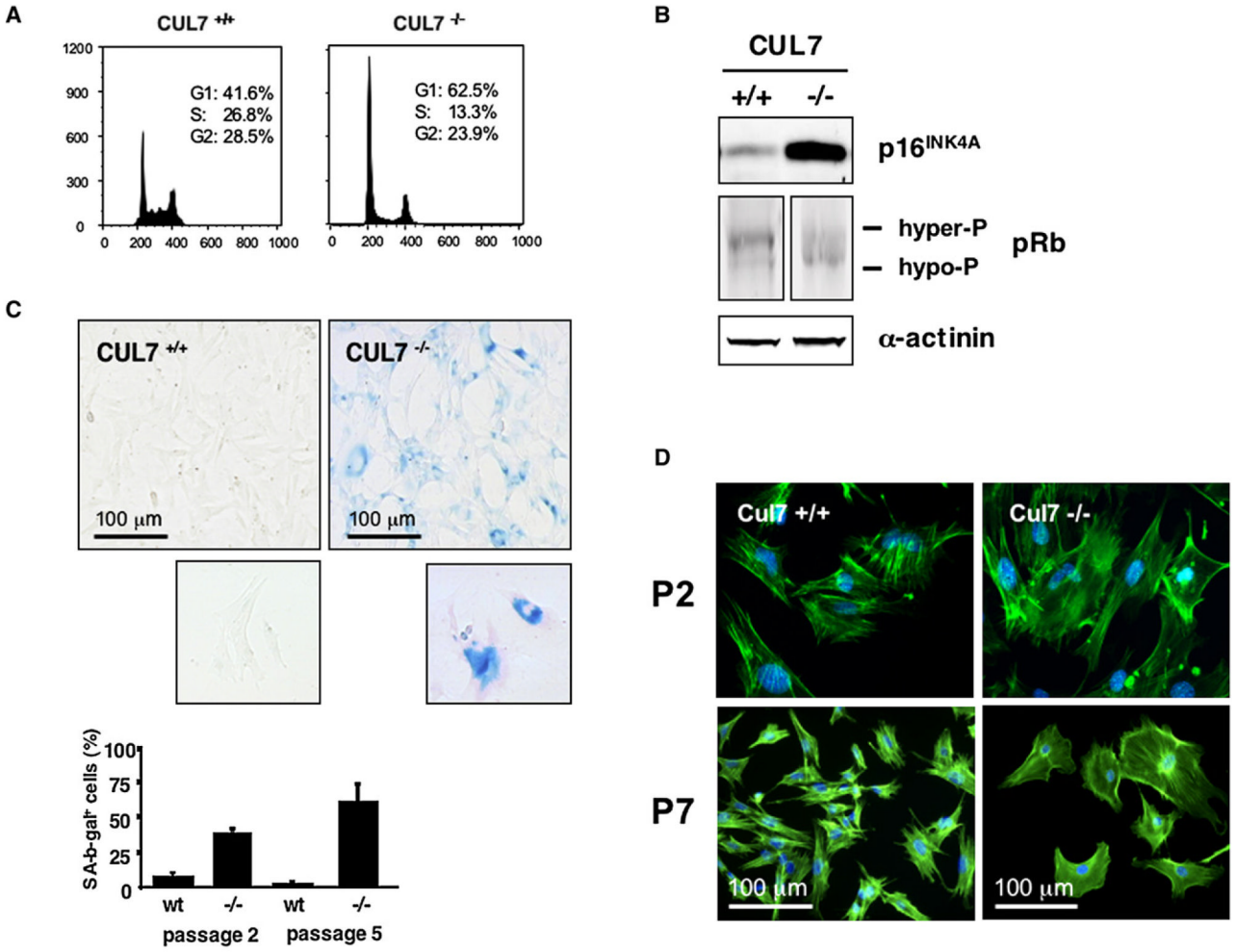

Figure 7. CUL7$^{-/-}$ MEFs Show Senescence Phenotypes

(A) *CUL7*$^{-/-}$ MEFs are G_1 arrested. Normal and *CUL7*$^{-/-}$ MEFs at passage 5 were analyzed by flow cytometry. Histograms of propidium iodide-stained cells are shown. The percentage of cells in G_1, S, and G_2/M phases of the cell cycle is indicated.

(B) *CUL7*$^{-/-}$ MEFs induce p16 and exhibit hypophosphorylated pRb. Extracts (100 μg of protein) from normal or *CUL7*$^{-/-}$ MEFs at passage 5 were subject to immunoblot analysis to monitor the levels of p16, pRb, and α-actinin (as a control for equal loading).

(C) *CUL7*$^{-/-}$ MEFs exhibited elevated levels of β-gal activity. Normal and *CUL7*$^{-/-}$ MEFs were stained for senescence-associated β-gal activity using a protocol as described (Serrano et al., 1997). Top and bottom panels show photographs of the normal and *CUL7*$^{-/-}$ MEFs at 100× and 400× magnification, respectively. β-gal-positive *CUL7*$^{+/+}$ and *CUL7*$^{-/-}$ MEFs at passage 2 and 5 were quantitated and shown graphically. Note that the graph integrates the results of three independent experiments, with error bars for the calculated standard deviation.

(D) Cell morphology of *CUL7*$^{+/+}$ and *CUL7*$^{-/-}$ MEFs at passage 2 and 7. Morphology analysis was carried out as described in the Supplemental Data.